

Preliminary Conception and Test of Global Stability Decomposition for Flow Stability Analysis

Guohua Tu*, Qiang Yang*, Jianqiang Chen*** and Xianxu Yuan***
Corresponding author: ghtu@skla.cardc.cn

* State Key Laboratory of Aerodynamics, China Aerodynamics Research and Development Center, Mianyang 621000, China;

** Computational Aerodynamics Institute, China Aerodynamics Research and Development Center, Mianyang 621000, China.

Abstract: Global stability analysis can be applied to study the stability property of two- and three-dimensional inhomogeneous flows. However, traditional global stability analysis (matrix-form) is based on solving the eigenvalue problem of a huge matrix, which makes it inconvenient for users. Several matrix-free or Jacobian-free methods have been developed in recent years. These methods are usually more effective and convenient than the traditional one. With regard to the matrix-free methods, a Global Stability Decomposition (GSD) is developed in the present study. The GSD concerns with a series of initial disturbances and their companions after a small time interval evolution, namely the couples of $u'_i(t_0) \sim u'_i(t_0 + \Delta t)$. GSD produces modes each of which has a single frequency, growth rate and mode shape. Combined with high-order accurate CFD tools, GSD becomes an effective method in studying global linear instability of arbitrary base flows. The relations of GSD to dynamic mode decomposition and matrix-free method are also discussed.

Keywords: Global linear stability, Global stability decomposition, Flow stability, Jacobian-free method, Matrix-free method

1 Introduction

Flow instability studies can provide basic knowledge on many flow phenomena, such as flow separation and laminar-turbulent transition. Linear instability studies have been popular in fluid mechanics since the advent of classic Linear Stability Theory (LST), which mainly concerns with sinusoidal waves propagating in parallel or ‘locally’ parallel flows. For flows which are not strictly parallel but only vary slowly in streamwise direction, the methods by solving the Parabolized Stability Equations (PSE) are proven more accurate than the classic LST. However, for flow with multiple inhomogeneous spatial directions, neither classic LST nor PSE can produce accurate results.

Global stability theory[1][2] can be used to study the development of small-amplitude perturbations superposed upon steady or time-periodic flows, which may be inhomogeneous in two (Bi-Global) or three (Tri-Global) spatial directions. Global stability analysis generally needs to solve the eigenvalue problem of a huge non-symmetric sparse matrix, which makes the situation especially difficult for three-dimensional inhomogeneous flows. This puts forward the so-called ‘matrix-free’ methods [3]. Most ‘matrix-free’ methods convert the eigenvalue problem of a huge sparse matrix to the eigenvalue problem of a small matrix by some kinds of iteration methods, such as Arnoldi

iteration. No matter which kinds of methods are used, the global stability theory contains spatial discretization, which is nontrivial and has much influence on getting physically relevant results (global unstable modes). Thus high-order numerical methods with appropriate boundary conditions are necessary. Both the classic and the global linear instability analysis are concerned with a base flow. High-quality base flow is necessary because it provides the spatial variable coefficients of the underlying partial derivative eigenvalue/initial-value problem, and the results (modes) show the instability property of the base flow. Thanks to the rapid development of computational fluid dynamics (CFD), many CFD codes and software are available for computing base flows; some CFD tools are even high-order accurate. Beside base flow computation, can we also use these high-order accurate CFD tools in global stability analysis? Readers may find an answer from this study.

This paper proposes a mode decomposition method to find the global modes of least stable or most unstable temporal ones for arbitrary steady flows. This method can be used in combination with various high-order accurate CFD tools. Its relations to Dynamic Mode Decomposition (DMD)[4][5] and matrix-free method [6] are also given.

2 Global stability decomposition

Suppose an infinitely small disturbance \mathbf{u}' is added to a base condition \mathbf{u}_0 which generally satisfies some kinds of governing equations like Navier-Stokes equations. The evolution of the disturbance can be expressed by the following equation

$$d\mathbf{u}'/dt = \mathbf{A}\mathbf{u}', \quad (1)$$

where \mathbf{A} is the Jacobian matrix. A direct global stability analysis method is to solve the eigenvalue problem of $\mathbf{A}\boldsymbol{\varphi}_A = \lambda_A\boldsymbol{\varphi}_A$, where λ_A and $\boldsymbol{\varphi}_A$ are the eigenvalue and eigenvector of \mathbf{A} . However it is not easy to construct the matrix \mathbf{A} , and the size of \mathbf{A} is usually huge. Instead, we propose to march Eq. (1) by a small time interval Δt ,

$$\mathbf{u}'(t_0 + \Delta t) = \exp(\mathbf{A}\Delta t)\mathbf{u}'(t_0) \triangleq \mathbf{B}\mathbf{u}'(t_0), \quad (2)$$

where $\mathbf{B} \triangleq \exp(\mathbf{A}\Delta t)$. The eigenvalues and eigenvectors of \mathbf{A} and \mathbf{B} have the following relations

$$\lambda_A = \ln(\lambda_B) / \Delta t, \quad \boldsymbol{\varphi}_A = \boldsymbol{\varphi}_B. \quad (3)$$

The least stable or most unstable mode of \mathbf{A} usually corresponds to an inner eigenvalue with the largest real part. By applying Eq. (2), this most unstable mode of \mathbf{A} becomes the one of \mathbf{B} with largest absolute value, which is much easier to compute by iteration algorithms. We suggest to solve the eigenvalues of \mathbf{B} by orthogonal projection methods [7].

For a given series of initial small disturbances $\mathbf{u}'_1(t_0), \mathbf{u}'_2(t_0), \dots, \mathbf{u}'_m(t_0)$, and $\mathbf{u}'_i \neq k\mathbf{u}'_j$ if $i \neq j$ for any value of k , they form a subspace, $span\{\mathbf{u}'_1(t_0), \mathbf{u}'_2(t_0), \dots, \mathbf{u}'_m(t_0)\}$, and its matrix form $\mathbf{U}_m = [\mathbf{u}'_1(t_0), \mathbf{u}'_2(t_0), \dots, \mathbf{u}'_m(t_0)]$. We can generate the orthogonal basis \mathbf{v}_i of the subspace, and get the orthogonal matrix

$$\mathbf{V}_m = [\mathbf{v}_1, \mathbf{v}_2, \dots, \mathbf{v}_m], \quad (4)$$

where $\langle \mathbf{v}'_i, \mathbf{v}'_j \rangle = 1$ only for $i = j$; otherwise $\langle \mathbf{v}'_i, \mathbf{v}'_j \rangle = 0$. We can use Gram-Schmidt method to generate \mathbf{V}_m . Actually, it can also be obtained by the standard QR decomposition,

$$\mathbf{U}_m = \mathbf{Q}\mathbf{R}. \quad (5)$$

Then $\mathbf{V}_m = \mathbf{Q}$. Projecting \mathbf{B} into the subspace by orthogonal projection, we can get $\mathbf{V}_m^H \mathbf{B} \mathbf{V}_m$ whose eigen solutions are good approximation to parts of the eigen solutions of \mathbf{B} . Multiplying $\mathbf{V}_m^H \mathbf{B} \mathbf{V}_m$ by \mathbf{R}^{-1} and \mathbf{R} from the left and right side, respectively, we get an $m \times m$ small matrix \mathbf{S} ,

$$\mathbf{S} = \mathbf{R}^{-1} \mathbf{V}_m^H \mathbf{B} \mathbf{V}_m \mathbf{R} = \mathbf{R}^{-1} \mathbf{Q}^H \mathbf{B} \mathbf{Q} \mathbf{R} = \mathbf{R}^{-1} \mathbf{Q}^H \mathbf{B} \mathbf{U}_m. \quad (6)$$

\mathbf{S} is several orders smaller than \mathbf{B} . The eigenvalues and eigenvectors have the following relations

$$\lambda_B \approx \lambda_S, \quad \boldsymbol{\phi}_B = \mathbf{V}_m \mathbf{R} \boldsymbol{\phi}_S = \mathbf{U}_m \boldsymbol{\phi}_S. \quad (7)$$

However, \mathbf{B} is not easy to construct neither. Fortunately, \mathbf{B} is not necessary when we use Eq. (6) to compute the small matrix \mathbf{S} . Instead, we can use $\mathbf{B} \mathbf{U}_m$, which can be found from Eq. (2) as below

$$\mathbf{B} \mathbf{U}_m = [\mathbf{B} \mathbf{u}'_1, \mathbf{B} \mathbf{u}'_2, \dots, \mathbf{B} \mathbf{u}'_m] = [\mathbf{u}'_1(t_0 + \Delta t), \mathbf{u}'_2(t_0 + \Delta t), \dots, \mathbf{u}'_m(t_0 + \Delta t)]. \quad (8)$$

$\mathbf{u}'_i(t_0 + \Delta t)$ can be acquired by other methods, such as high accurate CFD methods or high fidelity experiments (e.g. PIV for fluid flows).

To summarize, the algorithm for solving the eigenvalue problem of the linear stability system (1) is as following:

Step 1: Set a series of initial disturbances \mathbf{U}_m .

Step 2: Time march Δt to get $\mathbf{B} \mathbf{U}_m = [\mathbf{u}'_1(t_0 + \Delta t), \mathbf{u}'_2(t_0 + \Delta t), \dots, \mathbf{u}'_m(t_0 + \Delta t)]$ by a high-order accurate CFD tool.

Step 3: Construct a small matrix \mathbf{S} by Eq. (6) where the \mathbf{Q} and \mathbf{R} matrices can be computed by a QR decomposition of \mathbf{U}_m .

Step 4: Compute the eigenvalues and eigenvectors of \mathbf{S} .

Step 5: Get the approximated eigenvalues and eigenvectors of \mathbf{A} by Eq. (7) together with Eq. (3)

This procedure can be regarded as mode decomposition of a series of disturbance pairs of $\mathbf{u}'_i(t_0) \sim \mathbf{u}'_i(t_0 + \Delta t)$, and the modes can denote the global stability properties of the base flow. We call this procedure as Global Stability Decomposition (GSD).

3 Initial disturbances and relations to other methods

3.1 Initial disturbances

The proposed GSD needs a series of initial small disturbances, $\mathbf{u}'_1(t_0), \mathbf{u}'_2(t_0), \dots, \mathbf{u}'_m(t_0)$, then march Δt to get $\mathbf{u}'_1(t_0 + \Delta t), \mathbf{u}'_2(t_0 + \Delta t), \dots, \mathbf{u}'_m(t_0 + \Delta t)$ by high-order accurate CFD tools. The first requirement when setting the initial disturbances is that any two initial disturbances are not parallel to each other. This requirement is easy to satisfy in CFD. From the view of nonparallel, orthogonal disturbances may be the best choice. From the view of getting physical-based modes, or to speed up the convergence rate, physical-based disturbances (such as acoustic waves, vortex waves, and Tollmien-Schlichting waves) may also be good choices. In this study, we tested orthogonal disturbances and random disturbances, and both can bring us reasonable global stability solutions. There is much freedom to set the initial disturbances, and future work is still necessary to investigate which kind of initial disturbances is the best.

The amplitude of the initial disturbance shall be small enough to validate the linear hypothesis, but still several orders larger than the system error (including round-off errors) of the CFD tools. Our suggestion is 10^{-8} - 10^{-3} of the base-flow values combined with double precision arithmetic.

3.2 Relations to DMD

DMD provides a means to decompose snapshots of flows into modes, with each mode having a single frequency and growth/decay rate. In DMD, one assumes a linear relationship between the snapshots

with

$$\mathbf{x}'_{i+j} = \mathbf{B}_{DMD}^j \mathbf{x}'_i. \quad (9)$$

Suppose $\mathbf{X}_1^m = [\mathbf{x}'_1, \mathbf{x}'_2, \dots, \mathbf{x}'_m]$, and $\mathbf{X}_2^{m+1} = [\mathbf{x}'_2, \mathbf{x}'_3, \dots, \mathbf{x}'_{m+1}]$, then

$$\mathbf{X}_2^{m+1} = \mathbf{B}_{DMD} \mathbf{X}_1^m. \quad (10)$$

The real part of an eigenvalue of \mathbf{B}_{DMD} represents the growth/decay rate, whereas the image part indicates the frequency for the corresponding eigenvector (DMD mode) of \mathbf{B}_{DMD} .

In the present GSD, the initial disturbances can be generated by Arnoldi procedure, which means we only need to set one initial disturbance, and the others can be computed by

$$\mathbf{u}'_{1+i}(t_0) = \mathbf{u}'_1(t_0 + i\Delta t) = \mathbf{B}^i \mathbf{u}'_1(t_0). \quad (11)$$

Actually, we can use high-order accurate CFD methods to time-march $i\Delta t$ from the first initial disturbance $\mathbf{u}'_1(t_0)$ to get $\mathbf{u}'_{1+i}(t_0)$. Then, a series of initial disturbances and their corresponding disturbances after Δt can be rewritten in a matrix form as

$$\mathbf{U}_m = [\mathbf{u}'_1(t_0), \mathbf{B}^1 \mathbf{u}'_1(t_0), \dots, \mathbf{B}^{m-1} \mathbf{u}'_1(t_0)] \text{ and } \mathbf{B}\mathbf{U}_m = [\mathbf{B}^1 \mathbf{u}'_1(t_0), \mathbf{B}^2 \mathbf{u}'_1(t_0), \dots, \mathbf{B}^m \mathbf{u}'_1(t_0)]. \quad (12)$$

In this case, GSD is equivalent to DMD by setting $\mathbf{X}_1^m = \mathbf{U}_m$, and naturally

$$\mathbf{X}_2^{m+1} = [\mathbf{B}^1 \mathbf{u}'_1(t_0), \mathbf{B}^2 \mathbf{u}'_1(t_0), \dots, \mathbf{B}^m \mathbf{u}'_1(t_0)] = \mathbf{B}\mathbf{X}_1^m. \quad (13)$$

Then, we can find that DMD, if applied to analyze global instabilities of a steady base flow, is a special case of GSD where the initial disturbances are generated by Arnoldi procedure.

3.3 Relations to matrix-free method

The matrix-free (or Jacobian-free) method is a time-stepping approach for the approximate solution of global modes. Gómez et al. [6] gave an excellent example to demonstrate the powerfulness of the method. Our method is similar to the Jacobian-free method given in [6] and the references therein in three aspects: First, both of the methods do not need to construct an explicit Jacobian matrix; Second, both need to use a CFD tool; Third, both produce the approximate solution of the exact global modes. However, the present GSD is different from the matrix-free method in two aspects: First, there is more freedom in the present method when setting the initial disturbances, which makes it more convenient to use; Second, it is not necessary in GSD to use the Fréchet derivative to compute $e^{A\tau} \mathbf{u}'$, instead, the GSD directly use a series of $\mathbf{u}'_i(t_0)$ and the numerical result $\mathbf{u}'_i(t_0 + \Delta t)$ to form a small matrix by Eq. (6) in combination with QR decomposition.

4 Validation cases

Three testing cases, *i.e.*, one-dimensional incompressible Poiseuille flow, two-dimensional square cylinder and circular cylinder wake flows, are investigated to validate the proposed GSD method.

4.1 One-dimensional Poiseuille flow

The CFD solver used for this study is *Diablo*, which is an open source software developed by Bewley [8]. For Poiseuille flow, the solver uses Fourier series with 2/3 dealiasing rule for the streamwise and spanwise directions, and second-order central difference for the wall-normal direction. During the simulation, the mass flow rate is kept constant. The Reynolds number based on the centerline velocity and half channel height h is $Re = 10000$. To capture small disturbances in wall-normal direction, 129 points are used in this direction, with a hyper-tangential stretching parameter of 1.75 to make the

near-wall region better resolved. The domains size and grid points are $[2\pi h, 2h, h]$ and $[4, 129, 2]$ in streamwise, wall-normal and spanwise directions, respectively. Refer to [9], the constructed flow system resolves only two wall-parallel modes, *i.e.*, streamwise and spanwise wave number $(\alpha, \beta) = (0, 0)$ and $(\alpha, \beta) = (1, 0)$. The base flow is the analytic parabolic profile, *i.e.*, $U = 1 - y^2$.

We first add small amplitude random disturbances to the base flow. Because random disturbances cannot satisfy the governing equations of fluid flows, there must be a self-modulation period. After a short time of self-modulation process, the disturbance is supposed to satisfy the governing equation, and the disturbance is then normalized as a unit vector ξ_1 . The first initial disturbance is given as $\mathbf{u}'_1(t_0) = \varepsilon \xi_1$, where ε is the amplitude of disturbances. We can get $\mathbf{u}'_1(t_0 + \Delta t)$ by the CFD solver. Applying the Gram-Schmidt orthogonalization method to ξ_1 and $\mathbf{u}'_1(t_0 + \Delta t)$, we can get a unit vector ξ_2 , which is orthogonal to ξ_1 . Setting $\mathbf{u}'_2(t_0) = \varepsilon \xi_2$, we can get $\mathbf{u}'_2(t_0 + \Delta t)$ by the CFD tool. Continue with the Gram-Schmidt orthogonalization method, we can get a unit vector ξ_3 , which is orthogonal to the previous existing vectors $\{\xi_1, \xi_2\}$. We continue this procedure until the convergence of leading N eigenvalues. Usually, N can be a small number, e.g. 2, which means we only focus on the primary and secondary eigenvalues. For the amplitude of disturbances, we have tested $\varepsilon = 10^{-4}, 10^{-5}$, and 10^{-6} , and GSD results show that the amplitudes have little influence on the converged eigenvalues.

Figure 1 compares the eigen spectra between GSD and OS [9] (the method of directly solving the Orr-Sommerfeld equation). For the case of $Re = 10000$, there are two branches of eigenvalues, *i.e.*, the left branch and right branch in Figure 1. There is one eigen mode with a positive growth rate (unstable) on the left branch. All the other eigenvalues have negative real part (stable). The first 10 eigenvalues computed by GSD is in good agreement with the results in [9]. However, for the eigenvalues with small real parts, noticeable difference appears between the results of GSD and OS. The main reason for this discrepancy may be that the amplitudes of these modes are very small as they damp very fast, which means that these modes can be contaminated by CFD errors. Figure 2 compare the mode shape. For the primary mode and secondary mode, the GSD mode shapes are almost identical to the OS results [9]. Generally, the most important modes are the most unstable ones and least stable ones. GSD can accurately compute these modes. This case indicates that GSD is capable of studying one-dimensional stability problems, and the result is consistent with that of traditional temporal LST.

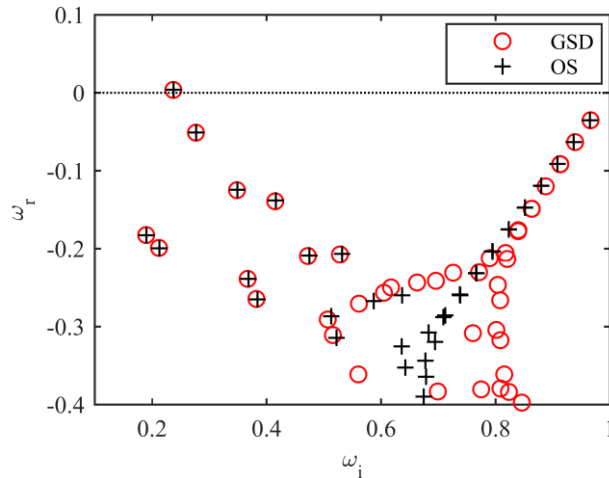


Figure 1 Leading eigenvalues from present GSD compared with OS result [9] for $Re=10000$ and $(\alpha, \beta) = (1, 0)$.

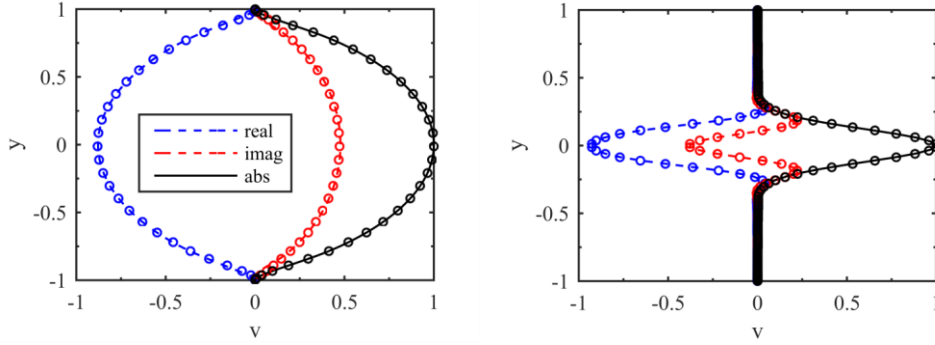


Figure 2 Mode shapes at $Re = 10000$ and $(\alpha, \beta) = (1, 0)$, shown by \hat{v} . Left: The most unstable mode (The leading mode on the left branch in Figure 1); Right: The least stable mode (The leading mode on the right branch in Figure 1). Symbols are from OS calculation [9], and lines are from present GSD.

4.2 Global unstable modes in the wake of a square cylinder

The second validation case is the flow over a square cylinder. One advantage of the present GSD is that the CFD tools can be changed without much adaption of the GSD code. In this section and the following section, we use an in-house high-order compressible flow code as the CFD solver. Details about the in-house code can be found in Ref. [11]-[16].

The flow conditions are similar to the one studied by Ohmichi & Suzuki [17]. The Mach number is 0.2, and five Reynolds numbers, *i.e.*, 40, 60, 80, 100, and 120 (based on the length of the square side d) are studied. The outflow boundary is located at $150d$ downstream of the square to minimize the boundary effect. In order to get a steady base flow, the flow is forced to be symmetric along the symmetry line, *i.e.*, $v|_{y=0} = 0$. Whereas the symmetry condition is switched off when computing the evolution of disturbances. The base flow for $Re=120$ is shown in Figure 3.

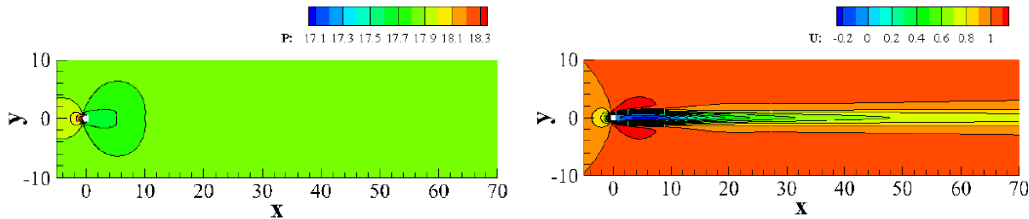


Figure 3 Base flow for square cylinder at $Re=120$. Left: pressure; Right: streamwise velocity.

The initial disturbances are given by the same method as in the previous subsection, which start from random disturbances and Gram-Schmidt method is applied to generate a sequence of orthogonal disturbances. There are a primary wake (PW) mode and a secondary wake (SW) mode. The PW mode becomes unstable as the Reynolds number approximately greater than 45, and the SW mode becomes unstable as the Reynolds number approximately greater than 96 [17]. The growth rates of the PW and SW modes are given in Figure 4. When considering the PW mode, our result is in good agreement with that in Ref. [17]. However, when considering the SW mode, the agreement with Ref. [17] is less satisfactory, especially at high Reynolds numbers. The small discrepancy between the present results and those in Ref. [17] may attribute to the difference in boundary treatment. Theofilis [1] pointed out that inflow and outflow boundary conditions for open flows needs further studying, especially for

flows involving (hydrodynamic or aeroacoustic) wave propagation. The outflow and far field boundary conditions in the present computing are closed by supposing Riemann invariants, which are widely used in engineering CFD. This boundary closure is robust for steady flows. However, for wave propagation, it may cause serious reflections and fake oscillations in the vicinity of boundaries. Ohmichi & Suzuki [17] tested three kinds of boundary treatments, and all the treatments are more suitable for wave propagation than ours. The SW mode is more difficult to compute as it extends very long in the wake, which makes it more likely to be affected by outflow boundary conditions. Both PW mode and SW mode at $Re = 120$ are shown in Figure 5, which also shows the result of Ohmichi & Suzuki [17] for comparison, and a qualitative agreement is achieved.

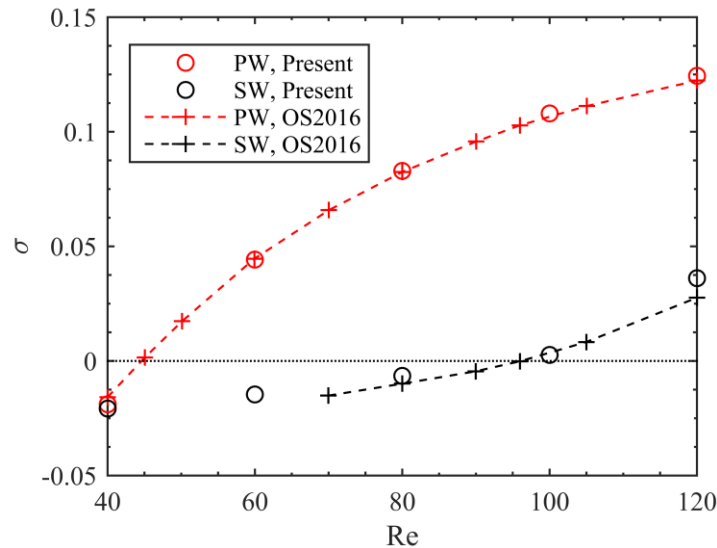


Figure 4 Growth rates of the global stability modes in the wake of a square cylinder. OS2016 denotes the results computed by Ohmichi & Suzuki [17].

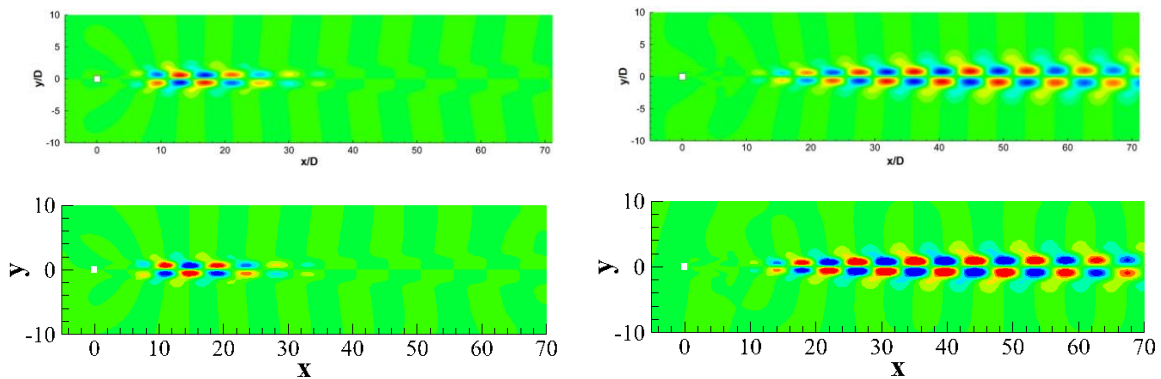


Figure 5 Shapes of the PW (left) and SW (right) modes (shown by the real part of streamwise velocity). Upper: Results of Ohmichi & Suzuki [17]. Lower: Present result.

4.3 Global unstable modes in the wake of a circular cylinder

The wake stability property of a smooth circular cylinder is similar to that of the previous square cylinder. Both cylinders have a PW mode and a SW mode. For wake flow behind a circular cylinder with Reynolds number greater than 46.9, the PW mode shall be unstable [18]. When the Reynolds number is greater than 110.8, the SW mode shall also be unstable [18]. If the Reynolds number is less than 180, the flow may still remain two-dimensional, but Karman vortex shedding is expected to appear. Beyond Reynolds number 180, more complicated phenomena may be observed in the wake,

such as spanwise undulation and laminar-turbulent transition.

Two sets of grids are used, *i.e.*, Grid I and Grid II as shown in Figure 6. The outflow boundary of Grid I is at $x = 30$ (in reference to cylinder center and non-dimensionalized by the cylinder diameter). The grids from $x = 20$ to $x = 30$ are stretched for the purpose of reducing boundary reflection. Thus the effective domain is cut off at $x=20$. The domain of Grid II is larger than Grid I, with outflow boundary at $x = 60$, and the effective domain cut off at $x = 40$. Numerical tests shows that Grid I is too small, which makes the computed results slightly oscillatory. Grid II is large enough for the convergence of the primary and secondary eigenvalues. The results below are based on Grid II.

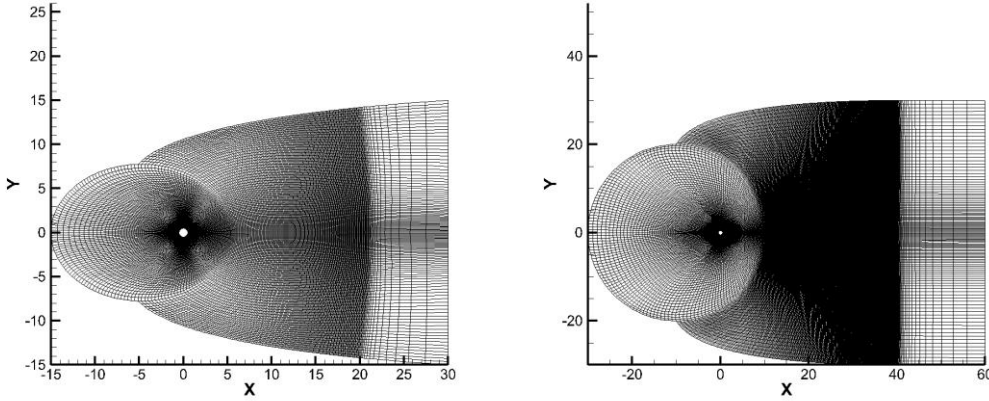


Figure 6 Grids for circular cylinder wake flow. Left: Grid I; Right: Grid II.

The flows with Reynolds numbers 100 and 150 are tested. The selective frequency damping (SFD) method [20] is applied when computing the base flow. The SFD method helps us in getting steady base flows, while the symmetry conditions used in the previous subsection fails when Reynolds number is 150. The base flows are shown in Figure 7. It is obvious that the separation bubble stretches its length as Reynolds number increases from 100 to 150. Barkley also shows the base flow for Reynolds number 100 (Figure 1c of Ref. [19]). Our result is identical to Barkley’s result.

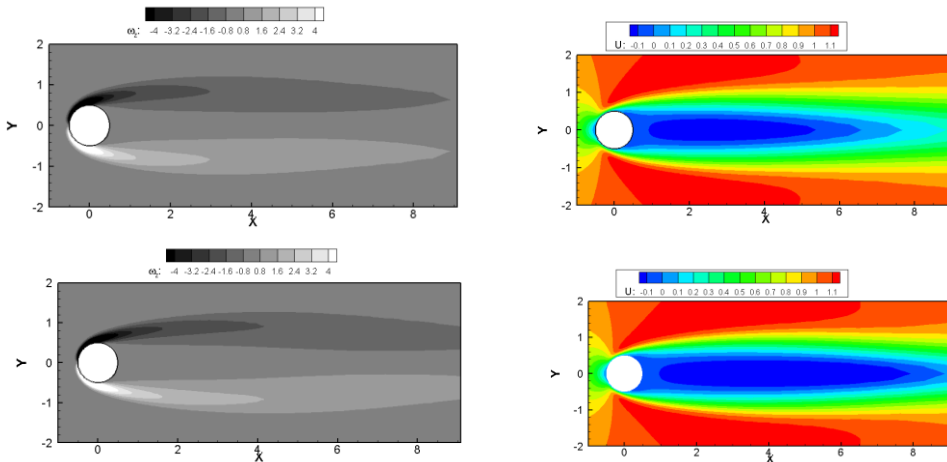


Figure 7 Base flows of circular cylinder. Upper: $Re=100$; Lower: $Re=150$. Left: $\omega_z = \partial v / \partial x - \partial u / \partial y$; Right: Streamwise velocity.

Three methods are used to produce initial disturbances for GSD. The first one is the same as the previous, namely starting with random disturbances, then continuing by the Gram-Schmidt method. The second method also starts with random disturbances, but the sequence of initial disturbances is

given by $u'_{i+1}(t_0) = u'_i(t_0 + \Delta t)$, which makes it equivalent to Arnoldi procedure. The second method is very simple, as users only need to record disturbance snapshots, *i.e.*, $u'_1(t_0)$, $u'_1(t_0 + \Delta t)$, ..., $u'_1(t_0 + m\Delta t)$, and perform GSD by setting

$$\begin{cases} \mathbf{U}_m = [u'_1(t_0), u'_1(t_0 + \Delta t), \dots, u'_1(t_0 + (m-1)\Delta t)], \\ \mathbf{BU}_m = [u'_1(t_0 + \Delta t), u'_1(t_0 + 2\Delta t), \dots, u'_1(t_0 + m\Delta t)]. \end{cases} \quad (14)$$

This procedure makes GSD similar to DMD. The third method to produce initial disturbances is the simplest one, *i.e.*, no disturbance is added to the base flow and disturbances appear by themselves, because unstable modes can grow from the system errors (such as round-off errors) of CFD tools. The only thing we need to do in the third method is to switch off the SFD after a steady base-flow state is obtained. Without the SFD, unstable disturbances grow from small amplitude (about 10^{-12}) exponentially. We start to record the disturbance snapshots when their amplitude is greater than 10^{-8} . These snapshots are put into Eq. (14) for the use of GSD. It shall be noted that second method may lead to unphysical modes, while the third method is only suitable for unstable modes, because stable modes cannot grow by themselves. Our test also shows that the three methods shows different convergence speeds. However, we have not done detailed investigation on convergence speed presently.

The vorticity of the PW mode at Reynolds 100 is shown in Figure 8, which also shows Barkley's result [19]. The streamwise velocity of the PW and SW modes at Reynolds 150 is shown in Figure 9, which also shows the result of Verma & Mittal [18]. Figures 8 and 9 show that, except a phase shift, our results are consistent with that of Ref. [19] and [18]. The phase shift is caused by the fact that eigenvectors can be arbitrarily translated and stretched. Figure 9 indicate that the SW mode extends further downstream compared to the PW mode, e.g. the SW mode is still visible in the domain of $x > 120$ (240 in Figure 9d). Although present computational domain is only effective for $x \leq 40$, GSD can still produce comparable results to that of Ref. [18], which indicate that another advantage of GSD is to produce good results on a relatively small computational domain.

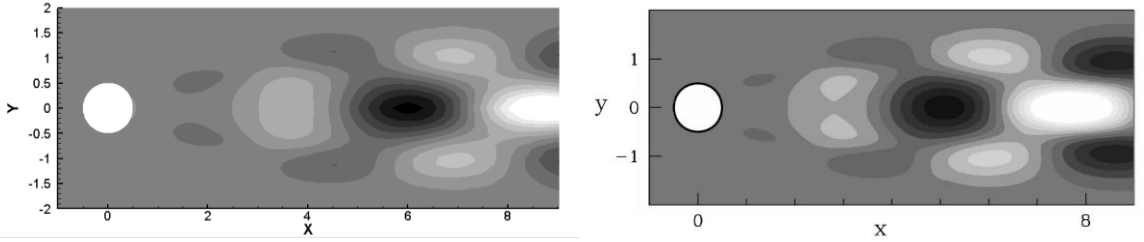
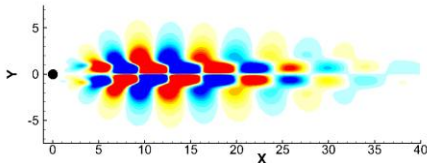
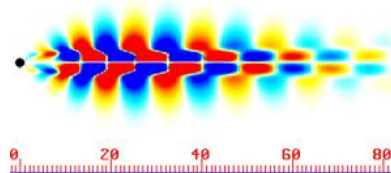


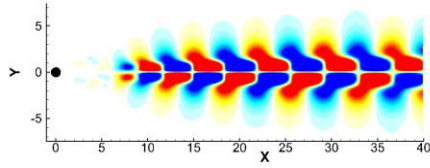
Figure 8 Vorticity of PW mode at $Re = 100$. left: Present result; Right: Barkley's result [19].



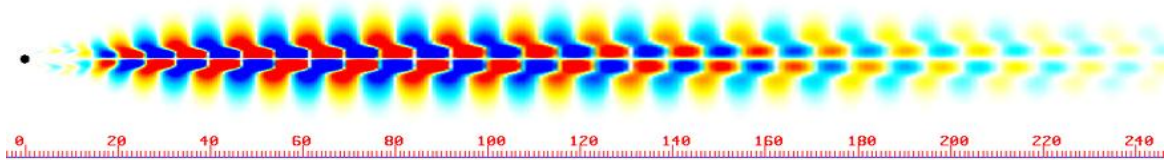
(a) PW mode, present result.



(b) PW mode, Verma & Mittal's result [18].



(c) SW mode, present result.



(d) SW mode, Verma & Mittal's result [18]

Figure 9 Streamwise velocity of PW and SW modes at $Re = 150$. Reference lengths are cylinder diameter for present results and cylinder radius for Verma & Mittal's results, respectively.

The growth rate and frequency of the PW and SW modes are shown in Figure 10. Several results from literature are also shown in Figure 10. Our result is most close to Verma & Mittal's result [18]. The largest difference between present result and that of Ref. [18] exist in the SW mode at $Re = 150$. Present growth rate is 9.7% lower, and present frequency is 3.2% higher, when comparing to that of Ref. [18].

We can find that there is some difference among the results shown in Figure 10. This phenomenon indicates the difficulty in getting accurate global stability modes. From the literature, we know that the accuracy of global stability analysis is affected by at least the following factors: accuracy of base flows, accuracy of spatial discretization methods, boundary treatments, convergence degree of eigenvalues (if an iteration method is used), and computational domains.

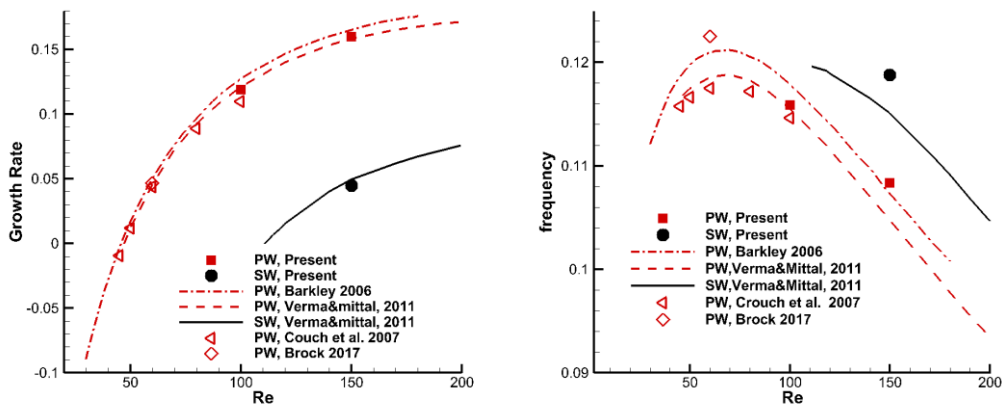


Figure 10 Growth rate and frequency of the PW and SW modes of the circular cylinder wake flow.

5 Conclusion and Future Work

A Global Stability Decomposition (GSD) method is proposed for the study of global linear stability of arbitrarily inhomogeneous flows. GSD can effectively decompose the leading eigen modes from a

series of disturbance pairs, $\mathbf{u}'_i(t_0) \sim \mathbf{u}'_i(t_0 + \Delta t)$, and each mode has a single frequency, growth/decay rate and mode shape. The disturbances $\mathbf{u}'_i(t_0)$ can be given by many methods (such as Gram-Schmidt procedure), provided that $\mathbf{u}'_i \neq k\mathbf{u}'_j$ for any $i \neq j$. The $\mathbf{u}'_i(t_0 + \Delta t)$ can be computed by any high-order CFD tools for user's convenience. GSD is similar to DMD if the disturbances are generated by Arnoldi method. Another advantage of GSD is that it can produce accurate global unstable modes on relatively small computational domains. Thus, GSD is user friendly and useful.

The results of three test cases show that GSD is capable of studying global linear stability of complex base flows. The three test cases are one-dimensional Poiseuille flow, the wake of a square cylinder and the wake of a circular cylinder. The computed GSD results are in consistence with the results of global linear stability analysis in literature.

Future work on setting initial disturbances and their influence on convergence speed is needed. Work on setting suitable Δt is also needed. It is expected that improved GSD can become an effective and accurate method in studying global linear instability of complex two- and three-dimensional incompressible and compressible (even hypersonic) flows in the near future.

References

- [1] V. Theofilis. Global linear instability. *Annual Review of Fluid Mechanics*, 43: 319–352, 2011.
- [2] F. Gómez, S. Le Clainche, P. Paredes, et al. Four decades of studying global linear instability: problems and challenges. *AIAA Journal*, 50(12): 2731-2743, 2012.
- [3] Gómez F, Pérez J M, Blackburn H M, Theofilis V. On the use of matrix-free shift-invert strategies for global flow instability analysis. *Aerospace Science and Technology*, 2015, 44: 69-76.
- [4] P. J. Schmid. Dynamic mode decomposition of numerical and experimental data. *Journal of Fluid Mechanics*, 656: 5-28, 2010.
- [5] C. W. Rowley, I. Mezić, S. Bagheri, et al. Spectral analysis of nonlinear flows. *Journal of Fluid Mechanics*, 641(1): 115-127, 2009.
- [6] F. Gómez, R. Gómez, V. Theofilis. On three-dimensional global linear instability analysis of flows with standard aerodynamics codes. *Aerospace Science and Technology*, 32: 223-234, 2014.
- [7] R. A. Horn and C. R. Johnson. *Matrix Analysis* (Second Edition). Cambridge University Press, 2013.
- [8] T. R. Bewley. *Numerical renaissance: simulation, optimization, & control*. Renaissance Press, 2014.
- [9] M. P. Juniper, A. Hanifi and V. Theofilis. Modal stability theory. *Applied Mechanics Review*, 66(2): 024804, 2014.
- [10] A. Tezuka and K. Suzuki. Three-dimensional global linear stability analysis of flow around a spheroid. *AIAA Journal*, 44(8): 1697-1708, 2006.
- [11] X. Deng, M. Mao, G. Tu, et al. High-order and high accurate CFD methods and their applications for complex grid problems. *Communication in Computational Physics*, 11(4): 1081-1102, 2012.
- [12] G. Tu, X. Deng, M. Mao. A staggered non-oscillatory finite difference method for high-order discretization of viscous terms. *ACTA Aerodynamica Sinica*, 29(1), 10-15, 2011.
- [13] G. Tu, X. Deng, M. Mao. Spectral property comparison of fifth-order nonlinear WCNS and WENO difference schemes. *ACTA Aerodynamica Sinica*, 30(6): 709-712, 2012.
- [14] G. Tu, X. Deng, M. Mao. Implementing high-order weighted compact nonlinear scheme on patched grids with a nonlinear interpolation. *Computers and Fluids*, 77: pp. 181-193, 2013.
- [15] G. Tu, X. Zhao, M. Mao. et al. Evaluation of Euler fluxes by a high-order CFD scheme: shock instability. *International Journal of Computational Fluid Dynamics*, 28(5): 171-186, 2014.
- [16] G. Tu J. Chen, M. Mao, et al. On the splitting methods of inviscid fluxes for implementing high-order weighted compact nonlinear schemes. *Applied Mathematics and Mechanics*, 37(12): 1324-1344, 2016.

- [17]Y. Ohmichi and K. Suzuki. Assessment of global linear stability analysis using a time-stepping approach for compressible flows. *International Journal for Numerical Methods in Fluids*, 80: 614-627, 2016.
- [18]A. Verma and S. Mittal. A new unstable mode in the wake of a circular cylinder. *Physics of Fluids*, 23: 121701. 2011.
- [19]D. Barkley. Linear analysis of the cylinder wake mean flow. *Europhysics Letters*, 75(5): 750-756, 2006.
- [20]A. Kervik, E. Brandt, L. Henningson, et al. Steady solutions of the Navier-Stokes equations by selective frequency damping. *Physics of Fluids*, 18(6): 068102, 2006.
- [21]C. K. W. Tam and J. C. Webb. Dispersion-relation-preserving finite difference schemes for computational acoustics. *Journal of Computational Physics*, 107:262–281, 1993.
- [22]J. M. Brock. Development of modal analysis for the study of global modes in high speed boundary layer flows. PhD thesis, the University of Minnesota, May 2017.